The Journal of Physical Chemistry Letters 9.4 (2018): 756-762

DOI: http://doi.org/10.1021/acs.jpclett.7b03220

Electron correlation in the ionization continuum of molecules: photoionization of N_2 in the vicinity of the Hopfield series of autoionizing states

Markus Klinker,[*,†] Carlos Marante,[†] Luca Argenti,[†,§] Jesús González-Vázquez,[*,†] and Fernando Martín[*,†,‡,¶]

Departamento de Química, Módulo 13, Universidad Autónoma de Madrid, 28049 Madrid, Spain, EU, Instituto Madrileño de Estudios Avanzados en Nanociencia (IMDEA-Nanociencia), Cantoblanco, 28049 Madrid, Spain, EU, and Condensed Matter Physics Center (IFIMAC), Universidad Autónoma de Madrid, 28049 Madrid, Spain, EU

E-mail: markus.klinker@uam.es; jesus.gonzalezv@uam.es; fernando.martin@uam.es

[*]To whom correspondence should be addressed

[†]Departamento de Química, Módulo 13, Universidad Autónoma de Madrid, 28049 Madrid, Spain, EU

[‡]Instituto Madrileño de Estudios Avanzados en Nanociencia (IMDEA-Nanociencia), Cantoblanco, 28049 Madrid, Spain, EU

[¶]Condensed Matter Physics Center (IFIMAC), Universidad Autónoma de Madrid, 28049 Madrid, Spain, EU

[§]Current address: Department of Physics and CREOL College of Optics & Photonics, University of Central Florida, Orlando, Florida 32816, USA

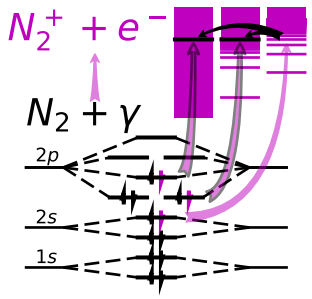

Abstract

Direct measurement of autoionization lifetimes by using time-resolved experimental techniques is a promising approach when energy-resolved spectroscopic methods do not work. Attosecond time-resolved experiments have recently provided the first quantitative determination of autoionization lifetimes of the lowest members of the well-known Hopfield series of resonances in N_2. In this work, we have used the recently developed XCHEM approach to study photoionization of the N_2 molecule in the vicinity of these resonances. The XCHEM approach allows us to describe electron correlation in the molecular electronic continuum at a level similar to that provided by multi-reference configuration interaction methods in bound state calculations, a necessary condition to accurately describe autoionization, shake-up and inter-channel couplings occurring in this range of photon energies. Our results show that, at variance with recent speculations, non-adiabatic effects play a minor role in this particular problem and that electron correlation is the main factor that determines the magnitude and shape of the N_2 photoionization cross sections, as well as the lifetimes of the Hopfield resonances. These conclusions are supported by the very good agreement between the calculated cross sections and those determined in synchrotron radiation and attosecond experiments.

The advent of attosecond light pulses has opened the way to perform time resolved measurements of electron dynamics in atoms and molecules, thus allowing one to reach the ultimate frontier responsible for chemical bonding.[1–5] The attosecond time resolution provided by these novel light sources has permitted, among other accomplishments, to determine the lifetimes of atomic autoionizing states from the direct observation of their exponential decay with time.[1,6] For isolated resonances, the lifetimes resulting from such measurements are in perfect agreement with those obtained from photoelectron spectra obtained in synchrotrons. However, when resonances overlap in the spectral domain, the usual situation in molecules when several ionization threshold are accessible, extraction of the corresponding lifetimes from such spectra is not so straightforward, and a direct time resolved measurement could be a better alternative, especially when the lifetimes are substantially different.[5]

A common characteristic of all attosecond measurements, which is also shared with synchrotron radiation measurements, is that ionization is produced by absorption of a single XUV or X-ray photon. In addition to direct ionization, where a single electron takes the excess of photon energy, a variety of processes in which this energy is shared between two or more electrons can also occur: inner-shell ionization followed by Auger decay, autoionization from Rydberg or multiply excited states, ionization accompanied by excitation of the remaining ion (shake up), Auger decay in combination with shake up, inter-channel couplings between different ionization continua, etc.[1] All these processes are mainly governed by electron correlation.

Recently, attosecond XUV-pump / IR-probe experiments have been performed to determine, for the first time, the lifetimes of molecular autoionizing states,[7] namely of the lowest members of the Hopfield[8,9] series of autoionizing states in the N_2 molecule. These states lie above the second ionization threshold of N_2 and, therefore, can autoionize by emitting an electron and leaving N_2^+ in either the ground or the lowest excited state (shake up). Furthermore, the lowest members of the series lie only a few hundreds of meV above the threshold, so that they can autoionize by emitting a rather slow electron, which can therefore strongly interact with the electrons remaining in the molecular cation (inter-channel coupling). A conspicuous result of these measurements is the large

differences in the autoionizing lifetimes of two of these series (one with much longer lifetimes than the other). This was tentatively attributed in Ref. 10 to interference stabilization between nearly degenerate Rydberg states, and more specifically in Ref. 11 to non-adiabatic rotational couplings between these states. However, there is no direct experimental or theoretical proof that this is indeed the reason for the differences in the observed lifetimes.

The Hopfield series has also been investigated by using synchrotron radiation.[12–16] Although the total photoelectron spectra resulting from these earlier experiments are qualitatively similar to the most recent time-resolved ones, the shape and assignment of the resonance peaks are significantly different. Furthermore, the lack of experimental information on the partial photoionization cross sections and on molecular orientation, as well as the fact that many of these resonances overlap in the same spectral region, has prevented synchrotron radiation measurements from providing the lifetimes for the lowest Hopfield resonances. Therefore, the accuracy of the lifetimes reported in such attosecond measurements, which are benchmark for similar applications of attosecond technology to more complicated molecules, remains to be checked.

An accurate theoretical description of N_2 photoionization in this energy region is only possible by appropriately describing electron correlation in the molecular continuum. This is a challenge for most existing theoretical methods, which have thus mainly focused on the description of the direct ionization process at different levels of approximation.[17–19] To our knowledge, the only existing theoretical calculations of N_2 photoionization that account for the lowest members of the Hopfield series were performed as early as in 1983[20] and 1991[21] by using multichannel quantum defect theory (MCQDT) and multichannel frozen-core Hartree-Fock approximation (MCFCHF), respectively. At that time, only an approximate description of the various matrix elements that enter either the MCQDT or the MCFCHF equations was possible (frozen-core, static exchange and single-centre continuum approximations, among others), so that they cannot be used as reference for the measured autoionization lifetimes. Thus, in spite of the apparent simplicity of the N_2 molecule, a precise understanding of its correlated ionization dynamics is still to be achieved. Getting an accurate description of multichannel resonant ionization in this fundamental system is a prerequisite

to understand correlation-induced ionization processes in more complicated molecules. In particular, autoionizing Auger decay has been identified as an important cause of molecular damage in biological systems.[22]

In this work, we have evaluated the photoionization spectrum of N_2 between the second and the third ionization thresholds within the adiabatic approximation by using the recently proposed XCHEM[23] code, which includes electron correlation in the electronic continuum at the same level as the most advanced quantum chemistry methods do for bound states. Except very close to threshold, the calculated total photoionization spectrum is in excellent agreement with the most recent spectra obtained with synchrotron radiation, and the calculated resonance lifetimes are very close to those determined in synchrotron radiation experiments and of the order of those obtained from the attosecond pump-probe experiments mentioned above. From these calculations, we conclude that the large differences in the lifetimes of the different states that compose the Hopfield series are almost entirely due to differences in electron correlation and not to non-adiabatic rotational effects as claimed in earlier work. From the analysis of the partial photoionization cross sections, we show that the dominant ionization channel leaves the N_2^+ ion in the $^2\Pi_u$ excited state, not in the $^2\Sigma_g^+$ ground state, and that the overall shape of the resonances observed in the total photoionization spectrum is mainly due to molecules oriented parallel to the polarization direction of the electric field.

We start by briefly describing the methodology used in the present work. In the XCHEM approach, the N_e-electron continuum wave function $\Psi^-_{\alpha E}$ is written as the close-coupling (CC) expansion

$$\Psi^-_{\alpha E}(\mathbf{x}_1,\cdots,\mathbf{x}_{N_e}) = \sum_i \aleph_i(\mathbf{x}_1,\cdots,\mathbf{x}_{N_e})c_{i,\alpha E} + \sum_{\beta i} N_{\beta i}\hat{\mathscr{A}}\Upsilon_\beta(\mathbf{x}_1,\cdots,\mathbf{x}_{N_e-1},\hat{\mathbf{x}}_{N_e})\phi_i(r_{N_e})c_{\beta i,\alpha E}, \quad (1)$$

where the first term includes the so-called short range states $\aleph_i$, in which all electrons reside within a radius R_0, and the second term contains anti-symmetrized products between one-electron radial continuum functions $\phi_i(r_N)$ and (N_e-1)-electron channel functions $\Upsilon_{\beta i}$. The latter represent an

(N_e-1)-electron parent ion state Φ_b multiplied by the angular part of the N_e-th (continuum) electron (X_{lm}) and coupled to the spin (χ) of the latter electron, so as to leave the N_e-electron system in a state of well defined total spin S and z-component Σ. Hence, every Υ_β can be unambiguously identified by the channel index $\beta = \{b, l, m, S, \Sigma\}$. The utility of this approach becomes apparent upon observing that, among the terms appearing in equation 1, only $\phi(r_{N_e})$ extends beyond R_0, which is essential to impose the appropriate incoming-wave boundary conditions of continuum wave functions for the photoionization problem. All other terms can thus be computed by using the tools of quantum chemistry packages (QCP) by expressing both short-range $\aleph_i$ and parent-ion Φ_b states in terms of orbitals represented by Gaussian basis functions ($G_i^P(r)$) centered at the atomic sites of the molecular system. In this work we have carried out state-average Restricted Active Space SCF (SA-RASSCF) calculations by using the cc-pVQZ[24] basis set, allowing for all configurations in which the $1\sigma_{g/u}$ orbitals are doubly occupied, the $2\sigma_{g/u}$, $3\sigma_{g/u}$, $1\pi_{g/u}$ orbitals are occupied by any physically admissible number of electrons, and the $4\sigma_{g/u}$, $5\sigma_{g/u}$, $6\sigma_{g/u}$, $2\pi_{g/u}$, $3\pi_{g/u}$ and $1\delta_{g/u}$ orbitals contain at most two electrons (see Fig. 1a for notations). The state average was performed by optimizing the neutral states $X^1\Sigma_g^+$, $A^1\Pi_u$, $B^1\Sigma_u^+$ and $C^1\Sigma_u^+$. The RASSCF orbitals were computed with MOLPRO,[25] exploiting its capability to perform a state average calculation over states of different symmetry. All subsequent RASSCF calculations were performed with MOLCAS.[26]

To describe ϕ_i, we use a hybrid Gaussian and B-Spline (GABS)[27] basis placed at the center of mass of the molecule, with the B-Splines ($B_i(r)$) being non-zero for radii $> R_0$ and the Gaussians ($G_i^M(r)$) being nonzero for radii $< R_1$, such that $R_1 > R_0$. The Gaussian part of the GABS basis contains a set of 22 even-tempered functions $G_i^P(r) \propto r^{2k+l}e^{-\alpha_i r^2}$, with $\alpha_i = \alpha_0\beta^i$ ($\alpha_0 = 0.001$, $\beta = 1.46$, $i = 0, ..., 21$), $k \leq 2$ and $l \leq 3$. The B-Spline part is composed of a set of 390 B-Splines of order 7 extending from $R_0 = 7.0$ a.u. up to $R_{\max} = 200$ a.u.. The products in the second term of equation 1 were obtained by augmenting the parent ions Φ_b with orbitals expanded in the $G_i^P(r)$, $G_i^M(r)$ and $B_i(r)$ functions. The radius R_0 was chosen so that the condition $\langle B_i|G_j^P\rangle = 0$ is ensured for all polycentric Gaussian functions, thus drastically simplifying the

calculation of operator matrix elements,[23] in particular, the Hamiltonian matrix $\mathscr{H}$. Subsequently, physically relevant scattering states are constructed by fitting linear combinations of the eigenstates of $\mathscr{H}$ to the asymptotically correct expression of $\Psi^{-}_{\alpha E}$ enforcing photoionization boundary conditions.[23,27,28] In the present application, our close-coupling expansion includes all those channels that stem from the parent ions associated with the first three ionization thresholds (see Fig. 1). As a whole, the XCHEM approach allows us to exploit the flexibility and efficiency of QCPs by using polycentric Gaussians, and to use B-Splines for the long-range behavior of the continuum electron, all the while sidestepping many of the problems normally associated with the use of only Gaussians and/or B-Splines in molecular photoionization. For more details on the GABs basis, mathematical intricacies of the XCHEM approach as well as benchmark results, we refer to Refs. 23, 27, 29 and references therein.

Fig. 1 shows the energy positions and the ionization channels of N_2 in the region of interest. The Hopfield series of autoionizing states lie above the $A^2\Pi_u$ and below the $B^2\Sigma^+_u$ ionization thresholds, and is reached by photons with energy between 17.1 and 18.7 eV (the ionization potential of N_2 is 15.6 eV). Due to the dipole selection rule, only states of $^1\Sigma^+_u$ and $^1\Pi_u$ symmetries can be populated. For each symmetry and ionization threshold, an infinite number of channels is open, but their relative importance decreases with the value of the angular momentum of the ejected electron. Fig. 1 only shows the most relevant channels. As can be seen, the Hopfield states of $^1\Sigma^+_u$ symmetry have a dominant $2\sigma_u^{-1}ns\sigma_g$ or $2\sigma_u^{-1}nd\sigma_g$ character, and can decay to the ground state of N_2^+, $X^2\Sigma^+_g$, by ejecting an electron to the $\varepsilon p\sigma_u$ or the $\varepsilon f\sigma_u$ continua accompanied by de-excitation of one of the $3\sigma_g$ electrons to the $2\sigma_u$ orbital, or decay to the first excited state of N_2^+, $A^2\Pi_u$, by ejecting an electron to the $\varepsilon d\pi_g$ continuum accompanied by de-excitation of one of the $1\pi_u$ electrons to the $2\sigma_u$ orbital. Similarly, the states of $^1\Pi_u$ symmetry have a dominant $2\sigma_u^{-1}nd\pi_g$ character and can decay to the $X^2\Sigma^+_g$ state of N_2^+, by ejecting an electron to the $\varepsilon p\pi_u$ or the $\varepsilon f\pi_u$ continua accompanied by de-excitation of one of the $3\sigma_g$ electrons to the $2\sigma_u$ orbital, or decay to the $A^2\Pi_u$ state of N_2^+, by ejecting an electron to the $\varepsilon s\sigma_g$, $\varepsilon d\sigma_g$, or $\varepsilon d\delta_g$ continua accompanied by de-excitation of one of the $1\pi_u$ electrons to the $2\sigma_u$ orbital. For completeness, the

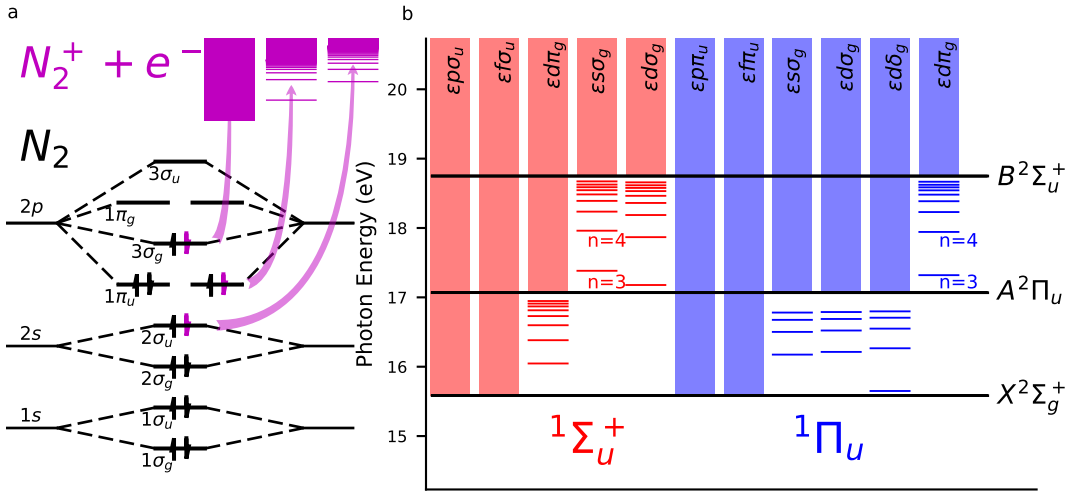

Figure 1: (a) Schematic representation of processes yielding different cationic states by removal of an electron from different molecular orbitals. The number preceding the symmetry notation for a particular molecular orbital indicates ordering within that symmetry. (b) Channels included in the CC expansion: five channels leave the systems in states of $^1\Sigma_u^+$ symmetry (red), and six in states of $^1\Pi_u$ symmetry (blue). The series of autoionizing states of interest to this work lie between the $A^2\Pi_u$ and $B^2\Sigma_u^+$ ionic states (corresponding to removing an electron from the $1\pi_u$ and $2\sigma_u$ molecular orbitals, respectively). These autoionizing states are indicated by two series of red ($ns\sigma_g$ and $nd\sigma_g$) and one series of blue ($nd\pi_g$) horizontal lines. Depending on the final symmetry of the system, these states may decay into either three or five open channels. In this panel, we have used the common united-atom limit notation introduced in Ref. 20 to label the excited electron.

energy diagram also shows the expected positions of the resonances lying between the first and the second ionization thresholds (i.e., below 17.1 eV). These resonances will not be investigated in the present work.

Fig. 2 shows the calculated total and partial photoionization cross sections obtained in both the length and velocity gauges. As can be seen, in all cases, the gauge invariance is very good. In Fig. 3, the calculated total cross sections are compared with the existing experimental results: the time-resolved measurements reported in Ref. 7 (panel a) and the earlier synchrotron radiation measurements in Refs. 13, 15, 16, 30 (panel b). For a meaningful comparison, in the latter figure the theory curves have been convoluted with a Gaussian function of width 0.03 eV (panel a) and 0.015 eV (panel b) to account for the limited energy resolution reported in the corresponding

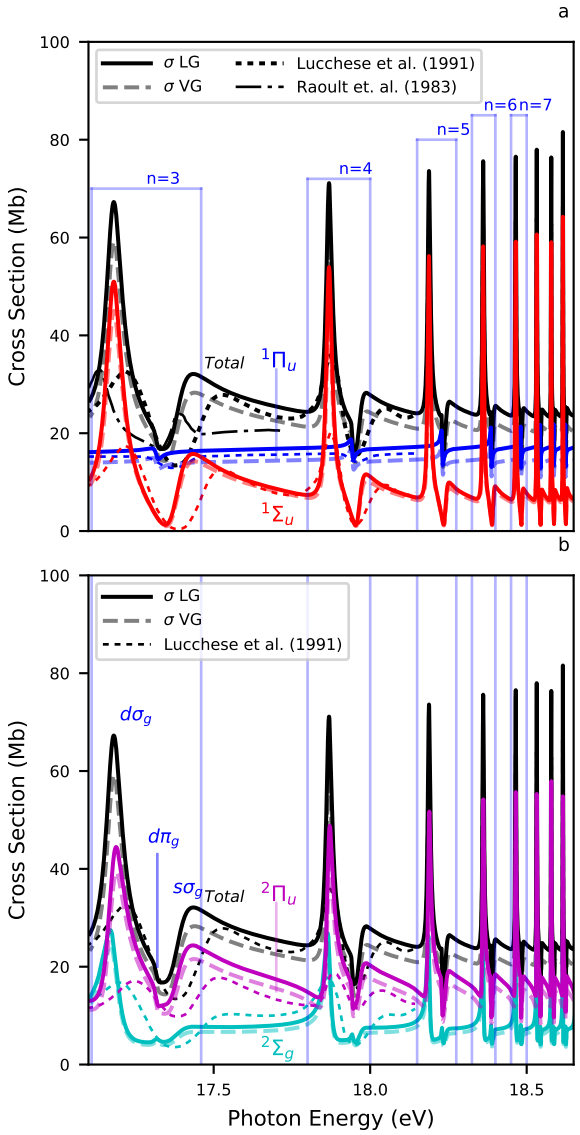

Figure 2: Total and partial photoionization cross sections of N_2. In both panels the black line corresponds to the total cross section and the colored lines to partial cross sections. Continuous lines: length gauge; dashed lines: velocity gauge. The dash-dotted and dotted lines are the theoretical results of Refs. 20 and 21, respectively. Panel (a) discriminates the cross section according to the symmetry of the N_e-electron system after ionization and clearly shows the relatively minor impact of the $nd\pi_g$ series on resonances. Panel (b) discriminates according to the (N_e-1)-electron parent ion left behind upon ejection of an electron, showing that after ionization it is more likely to find the ion in the excited $^2\Pi_u$ state than in the ionic ground state. This panel indicates the position of the lowest $3s\sigma_g$, $3d\sigma_g$ and $3d\pi_g$ resonances. For simplicity in the notation, in the text we have used the same index n for all resonances in the same group.

experiments. We also note that we have used the experimental ionization potential of N_2 but that no rescaling of the calculated cross section has been performed. As can be seen, the agreement

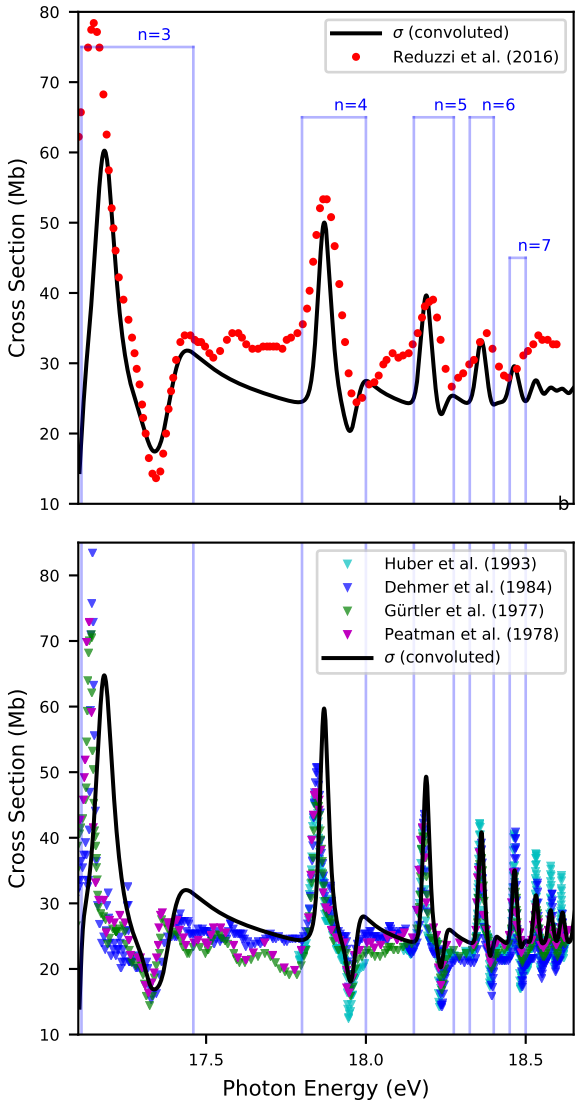

Figure 3: Comparison of the total photoionization cross section obtained using the XCHEM approach with (a) the attosecond measurements of Reduzzi et al[7] and (b) the synchrotron radiation measurements of Gürtler et al,[13] Peatman et al,[30] Dehmer et al,[15] and Huber et al.[16] Each blue box "contains" three resonance features according to the three series of autoionizing states diagrammatically shown in Fig.1b, collectively labelled by n.

between our calculated total cross sections and the synchrotron radiation data is very good in the whole range of photon energies, both in magnitude and shape, except for the lowest $2\sigma_u^{-1}3d\sigma_g$ resonance lying just above the $A^2\Pi_u$ threshold, which is slightly broader and is shifted to higher energies in the theoretical results. This might be due to an incorrect description of the electronic continuum just above threshold, where larger boxes are probably necessary, or to a breakdown

of the adiabatic approximation, since in this region the ejected electron is extremely slow and, therefore, has a velocity comparable to that of the nuclei. Interestingly, for this specific resonance, the agreement is slightly better when comparing with the time-resolved experimental results of Ref. 7 (see Fig. 3a). For all other resonances, including the other $(n = 3)$ ones, the agreement between calculated and experimental synchrotron radiation data is remarkable. As can be seen in Fig. 2, the shapes of these resonance peaks significantly differ from those reported in previous theoretical works.

The $^1\Sigma_u^+$ and $^1\Pi_u$ contributions to the total cross sections shown in Fig. 3a correspond, up to a factor, to the ionization cross sections of molecules oriented parallel and perpendicular to the polarization direction, respectively.[31,32] The analysis of these contributions reveals that almost all the features observed in the experimental spectra are exclusively due to resonances of $^1\Sigma_u^+$ symmetry, namely the $2\sigma_u^{-1}ns\sigma_g$ and $2\sigma_u^{-1}nd\sigma_g$ ones. These resonances show up as pronounced asymmetric peaks and dips, respectively, and barely overlap with each other, except for the upper and lower tails of the resonances with the same value of n. The peaks associated to the $2p\pi^{-1}nd\pi_g$ resonances, which show up in the $^1\Pi_u$ contribution, are very weak and have a characteristic asymmetric Fano profile. They are barely visible in the total photoionization cross sections and are well separated from each other. Therefore, in the absence of non-adiabatic effects, none of the above resonances are expected to interfere with each other. The good agreement between theory and experiment suggests, however, that non-adiabatic effects should play a minor role here, except maybe in the vicinity of the $2\sigma_u^{-1}3d\sigma_g$, which lies less than 100 meV above the $A^2\Pi_u$ threshold.

The partial cross sections of Fig. 2b show that, at these low photon energies, photoionization of N_2 leaves preferentially the N_2^+ cation in the $A^2\Pi_u$ excited state, instead of in the $X^2\Sigma_g^+$ ground state. In other words, direct and resonant ionization from the HOMO-1 dominates over direct and resonant ionization from the HOMO, with a possibly significant contribution from shake-up processes. Indeed, the rather large width of the Hopfield states is indicative of a strong coupling between different ionization channels in N_2.

Finally, from the calculated photoionization spectra, we have determined the energy positions

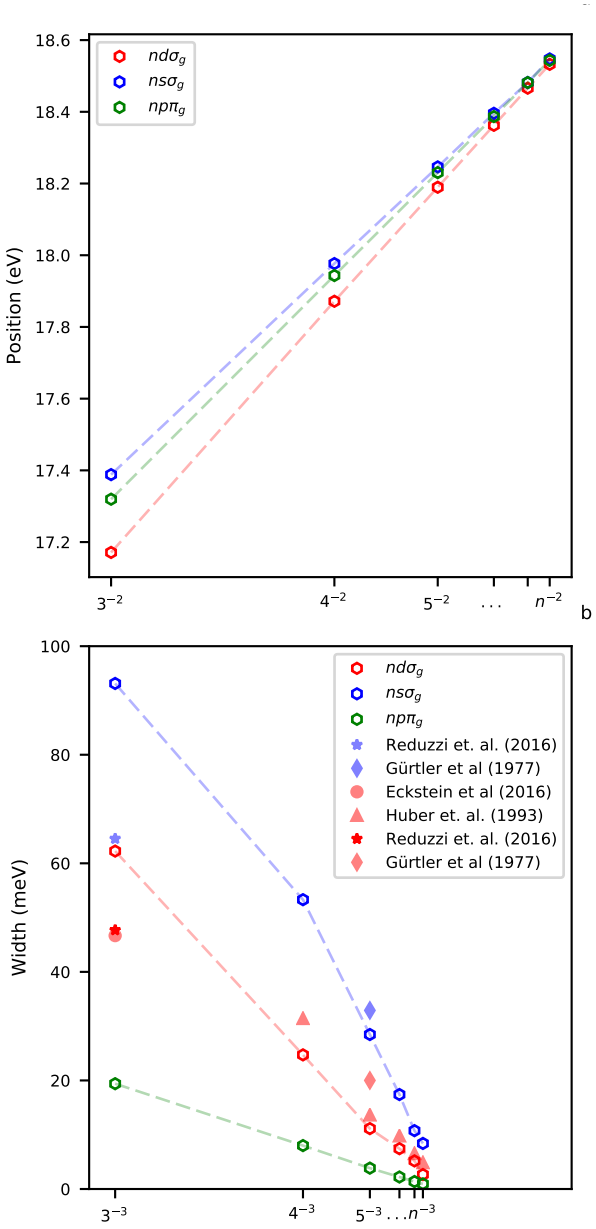

Figure 4: (a) Energies of the three relevant series of autoionizing states, extracted from the XCHEM results as outlined in the text ($ns\sigma_g$ in blue, $nd\sigma_g$ in red, $nd\pi_g$ in green). Clearly visible is the approximate n^{-2} scaling behavior. (b) The widths of the autoionizing states of panel (a), displaying an approximate n^{-3} scaling behavior. The XCHEM results are compared to reference data from synchrotron radiation measurements by Gürtler et al (1977)[13] and Huber et al (1993),[16] as well as to the 2016 time-resolved results from Reduzzi et al[7] and Eckstein et al,[10] the only ones available for the $3s\sigma_g$ and $3d\sigma_g$ resonances.

and autoionization widths of the three series of Hopfield resonances. This was done by fitting the computationally obtained data to the analytical expression[33] that describes the behavior of the

scattering phase in the vicinity of an autoionizing state,

$$\delta(E) = \delta_b + \tan^{-1}\frac{\Gamma_n}{2(E-E_n)}, \tag{2}$$

where E_n is the resonance position, Γ_n the resonance width and δ_b is a slowly varying background. The results thus obtained are shown in Fig. 4. The figure also includes the experimental values of the widths (i.e., the inverse of the lifetimes) determined in Refs 7, 10, 13, 16 for the $2\sigma_u^{-1}3s\sigma_g$ and $2\sigma_u^{-1}3d\sigma_g$ resonances. As in the atomic case, the energies and widths of the resonances of the three Hopfield series roughly scale as $1/n^2$ and $1/n^3$, respectively. Our calculated widths for $n \geq 4$ are in good agreement with those determined in the synchrotron radiation experiments of Refs 13, 16. For $n = 3$ the only available experimental data are those obtained from the time-resolved measurements of Refs. 7, 10. In this case, the calculated widths are significantly larger than the measured ones; however, their relative value ($\sim$1.5 for the $3d\sigma_g$ and $3s\sigma_g$ resonances) is in good agreement with the experimentally measured ratio. Therefore, the main finding of the time-resolved experiment of Ref 7, which is the significant difference in the lifetimes of these two resonances, is confirmed by the present calculations. Furthermore, Fig. 4 shows that a similar difference in magnitude is observed for all the members of the $2\sigma_u^{-1}ns\sigma_g$ and $2\sigma_u^{-1}nd\sigma_g$ series of resonances, thus confirming once again that the main reason for the different lifetimes is electron correlation, rather than non-adiabatic effects.

In conclusion, we have used the recently developed XCHEM approach to study photoionization of the N_2 molecule between the second and the third ionization thresholds, where the Hopfield series of autoionizing resonances show up. The XCHEM approach allows us to describe electron correlation for the electronic continuum at the same level of accuracy as multi-reference CI methods do for bound states. Our results show that non-adiabatic couplings play a minor role in this particular problem and that electron correlation is the main factor that determines the magnitude and shape of the N_2 photoionization cross sections, as well as the lifetimes of the Hopfield resonances. These conclusions are supported by the good agreement between the calculated cross

sections and those determined in early synchrotron radiation experiments and more recent attosecond measurements.

Acknowledgments

This work has been supported by the ERC advanced grant 290853 - XCHEM - within the seventh framework programme of the European Union and the MINECO projects FIS2013-42002-R and FIS2016-77889-R (AEI/FEDER, UE). We also acknowledge computer time from CCC-UAM and Marenostrum Supercomputer Centers. L.A. acknowledges support from the TAMOP NSF Grant No. 1607588, as well as UCF funding.

References

(1) Krausz, F.; Ivanov, M. *Rev. Mod. Phys.* **2009**, *81*, 163–234.

(2) Sansone, G. et al. *Nature* **2010**, *465*, 763–766.

(3) Calegari, F.; Ayuso, D.; Trabattoni, A.; Belshaw, L.; De Camillis, S.; Anumula, S.; Frassetto, F.; Poletto, L.; Palacios, A.; Decleva, P.; Greenwood, J. B.; Martín, F.; Nisoli, M. *Science* **2014**, *346*, 336–339.

(4) Kraus, P. M.; Mignolet, B.; Baykusheva, D.; Rupenyan, A.; Horný, L.; Penka, E. F.; Grassi, G.; Tolstikhin, O. I.; Schneider, J.; Jensen, F.; Madsen, L. B.; Bandrauk, A. D.; Remacle, F.; Wörner, H. J. *Science* **2015**, *350*, 790–795.

(5) Nisoli, M.; Calegari, F.; Palacios, A.; Decleva, P.; Martín, F. *Chem. Rev.* **2017**, *117*, 10760–10825.

(6) Drescher, M.; Hentschel, M.; Kienberger, R.; Uiberacker, M.; Yakovlev, V.; Scrinzi, A.; Westerwalbesloh, T.; Kleineberg, U.; Heinzmann, U.; Krausz, F. *Nature* **2002**, *419*, 803–7.

(7) Reduzzi, M.; Chu, W. C.; Feng, C.; Dubrouil, A.; Hummert, J.; Calegari, F. *Journal of Physics B* **2016**, *49*, 0.

(8) Hopfield, J. J. *Phys. Rev.* **1930**, *35*, 1133–1134.

(9) Ogawa, M.; Tankaka, Y. *Canadian Journal of Chemistry* **1962**, *40*, 1593.

(10) Eckstein, M.; Mayer, N.; Yang, C.-H.; Sansone, G.; Vrakking, M. J.; Ivanov, M.; Kornilov, O. *Faraday Discussions* **2016**, *194*, 509–524.

(11) Eckstein, M.; Yang, C.-H.; Frassetto, F.; Poletto, L.; Sansone, G.; Vrakking, M. J. J.; Kornilov, O. *Physical Review Letters* **2016**, *116*, 163003.

(12) Woodruff, P. R.; Marr, G. V. *Proceedings of the Royal Society A* **1977**, *358*, 87–103.

(13) Gürtler, P.; Saile, V.; Koch, E. E. *Chemical Physics Letters* **1977**, *48*, 245.

(14) Parr, A. C.; Ederer, D. L.; Cole, B. E. *Physical Review Letters* **1981**, *46*, 22.

(15) Dehmer, M. P.; Miller, P. J.; Chupka, W. A. *The Journal of Chemical Physics* **1984**, *80*, 1030.

(16) Huber, K. P.; Stark, G.; Ito, K. *The Journal of Chemical Physics* **1993**, *98*, 4471–4477.

(17) Bachau, H.; Cormier, E.; Decleva, P.; Hansen, J. E.; Martín, F. *Rep. Prog. Phys.* **2001**, *64*, 1815–1943.

(18) Toffoli, D.; Stener, M.; Fronzoni, G.; Decleva, P. *Chem. Phys.* **2002**, *276*, 25–43.

(19) Gozem, S.; Gunina, A. O.; Ichino, T.; Osborn, D. L.; Stanton, J. F.; Krylov, A. I. *The Journal of Physical Chemistry Letters* **2015**, *6*, 4532–4540.

(20) Raoult, M.; Le Rouzo, H.; Raseev, G.; Brion, L. H. *Journal of Physics B* **1983**, *16*, 4601.

(21) Lucchese, R. R.; Zurales, R. W. *Physical Review A* **1991**, *44*, 291–303.

(22) Howell, R. W. *Int. J. Rad. Biol.* **2008**, *84*, 959.

(23) Marante, C.; Klinker, M.; Corral, I.; González-Vázquez, J.; Argenti, L.; Martín, F. *Journal of Chemical Theory and Computation* **2017**, *13*, 499–514.

(24) Dunning Jr, T. H. *The Journal of chemical physics* **1989**, *90*, 1007–1023.

(25) Werner, H.-J.; Knowles, P. J.; Knizia, G.; Manby, F. R.; Schütz, M. *Wiley Interdisciplinary Reviews: Computational Molecular Science* **2012**, *2*, 242–253.

(26) Aquilante, F.; Autschbach, J.; Carlson, R. K.; Chibotaru, L. F.; Delcey, M. G.; De Vico, L.; Ferré, N.; Frutos, L. M.; Gagliardi, L.; Garavelli, M. *Journal of computational chemistry* **2016**, *37*, 506–541.

(27) Marante, C.; Argenti, L.; Martín, F. *Physical Review A* **2014**, *90*, 012506.

(28) Starace, A. F. *Fundamental Processes in Energetic Atomic Collisions*; Springer, 1982.

(29) Marante, C.; Klinker, M.; Kjellsson, T.; Lindroth, E. *Physical Review A* **2017**, 022507.

(30) Peatman, W. B.; Gotchev, B.; Guertler, P.; Seile, V.; Koch, E. E. *The Journal of Chemical Physics* **1978**, *69*, 2089–2095.

(31) Dill, D.; Dehmer, J. L. *The Journal of Chemical Physics* **1974**, *61*, 692–699.

(32) Dill, D. *The Journal of Chemical Physics* **1976**, *65*, 1130–1133.

(33) Hazi, A. U. *Physical Review A* **1979**, *19*, 920–922.